David Taylor Research Center

Bethesda, Maryland 20084-5000

DTRC-PAS-91/7 March 1991

Propulsion and Auxiliary Systems Dapartment

Research & Development Report

Unsteady Flows in Rotor-Stator Cascades

by
Yu-Tai Lee
Thomas W. Bein
Jin Zhang Feng
Charles L. Merkle

DTRC-PAS-91/7 Unsteady Flows in Rotor-Stator Cascades

DISCLAIMER NOTICE

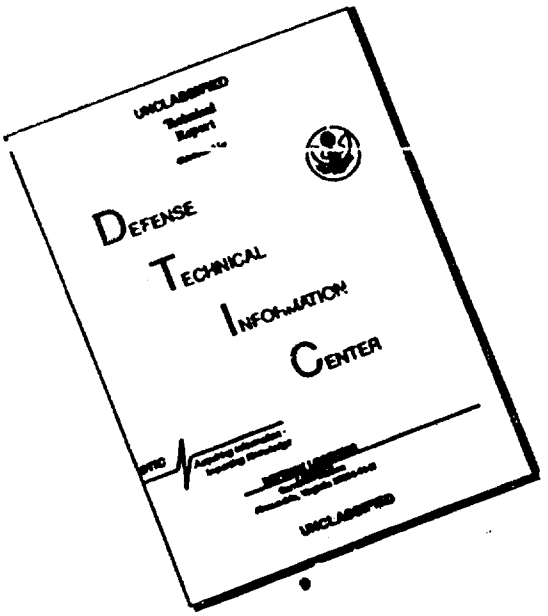

THIS DOCUMENT IS BEST QUALITY AVAILABLE. THE COPY FURNISHED TO DTIC CONTAINED A SIGNIFICANT NUMBER OF PAGES WHICH DO NOT REPRODUCE LEGIBLY.

MAJOR DTRC TECHNICAL COMPONENTS

CODE 011 DIRECTOR OF TECHNOLOGY, PLANS AND ASSESSMENT

12 SHIP SYSTEMS INTEGRATION DEPARTMENT

14 SHIP ELECTROMAGNETIC SIGNATURES DEPARTMENT

15 SHIP HYDROMECHANICS DEPARTMENT

16 AVIATION DEPARTMENT

17 SHIP STRUCTURES AND PROTECTION DEPARTMENT

18 COMPUTATION, MATHEMATICS & LOGISTICS DEPARTMENT

19 SHIP ACOUSTICS DEPARTMENT

27 PROPULSION AND AUXILIARY SYSTEMS DEPARTMENT

28 SHIP MATERIALS ENGINEERING DEPARTMENT

DTRC ISSUES THREE TYPES OF REPORTS:

1. **DTRC reports, a formal series,** contain information of permanent technical value. They carry a consecutive numerical identification regardless of their classification or the originating department.

2. **Departmental reports, a semiformal series,** contain information of a preliminary, temporary, or proprietary nature or of limited interest or significance. They carry a departmental alphanumerical identification.

3. **Technical memoranda, an informal series,** contain technical documentation of limited use and interest. They are primarily working papers intended for internal use. They carry an identifying number which indicates their type and the numerical code of the originating department. Any distribution outside DTRC must be approved by the head of the originating department on a case-by-case basis.

UNCLASSIFIED

SECURITY CLASSIFICATION OF THIS PAGE

REPORT DOCUMENTATION PAGE

Form Approved
OMB No 0704-0188

1a REPORT SECURITY CLASSIFICATION Unclassified	1b RESTRICTIVE MARKINGS
2a SECURITY CLASSIFICATION AUTHORITY	3 DISTRIBUTION/AVAILABILITY OF REPORT Approved for public release; distribution is unlimited.
2b DECLASSIFICATION/DOWNGRADING SCHEDULE	
4 PERFORMING ORGANIZATION REPORT NUMBER(S) DTRC-PAS-91/7	5 MONITORING ORGANIZATION REPORT NUMBER(S)
6a NAME OF PERFORMING ORGANIZATION David Taylor Research Center 6b OFFICE SYMBOL (If applicable) Code 2721	7a NAME OF MONITORING ORGANIZATION
6c ADDRESS (City, State, and ZIP Code) Annapolis, MD 21402	7b ADDRESS (City, State, and ZIP Code)
8a NAME OF FUNDING/SPONSORING ORGANIZATION Office of Naval Technology 8b OFFICE SYMBOL (If applicable, ONT 211 & 233	9 PROCUREMENT INSTRUMENT IDENTIFICATION NUMBER
8c ADDRESS (City, State, and ZIP Code) Arlington, VA 22217-5000	10 SOURCE OF FUNDING NUMBERS PROGRAM ELEMENT NO: 62121N, 62323N PROJECT NO TASK NO WORK UNIT ACCESSION NO
11 TITLE (Include Security Classification) Unsteady Flows in Rotor-Stator Cascades	
12 PERSONAL AUTHOR(S) Yu-Tai Lee, Thomas W. Bein, Jin Zhang Feng and Charles L. Merkle	
13a TYPE OF REPORT Phase 13b TIME COVERED FROM _____ TO _____	14 DATE OF REPORT (Year, Month, Day) March 1991 15 PAGE COUNT 34
16 SUPPLEMENTARY NOTATION	

17 COSATI CODES			18 SUBJECT TERMS (Continue on reverse if necessary and identify by block number)
FIELD	GROUP	SUB-GROUP	Unsteady potential flow, Lifting surface, Rotor, Stator, Interaction, Turbomachine

19 ABSTRACT (Continue on reverse if necessary and identify by block number)

A time-accurate potential-flow calculation method has been developed for unsteady incompressible flows through two-dimensional multi-blade-row linear cascades. The method represents the boundary surfaces by distributing piecewise linear-vortex and constant-source singularities on discrete panels. A local coordinate is assigned to each independently moving object. Blade-shed vorticity is traced at each time step. The unsteady Kutta condition applied is nonlinear and requires zero blade trailing-edge loading at each time. Its influence on the solutions depends on the blade trailing-edge shapes.

Steady biplane and cascade solutions are presented and compared to exact solutions and experimental data. Unsteady solutions are validated with the Wagner function for an airfoil moving impulsively from rest and the Theodorsen function for an oscillating airfoil. The shed vortex motion and its interaction with blades are calculated and compared to an analytic solution. For multi-blade-row cascade, the potential effect between blade rows is predicted using steady and quasi unsteady calculations. The accuracy of the predictions is demonstrated using experimental results for a one-stage turbine stator-rotor.

20 DISTRIBUTION/AVAILABILITY OF ABSTRACT ☒ UNCLASSIFIED/UNLIMITED ☐ SAME AS RPT ☐ DTIC USERS	21 ABSTRACT SECURITY CLASSIFICATION Unclassified
22a NAME OF RESPONSIBLE INDIVIDUAL Thomas W. Bein	22b TELEPHONE (Include Area Code) (301) 267-2159 22c OFFICE SYMBOL Code 2721

DD Form 1473, JUN 86 Previous editions are obsolete

S/N 0102-LF-014-6603

TABLE OF CONTENTS

FIGURES

FIGURES (continued)

NOMENCLATURE

C_L = lift coefficient

C_p = pressure coefficient

c = chord of the airfoil

CDU = velocity potential due to uniformly distributed vortex

CDL = velocity potential due to linearly distributed vortex

CD1 = coefficient defined in Eq. (12)

CD2 = coefficient defined in Eq. (12)

CS = coefficient defined in Eq. (12)

ds = small surface element

E = numerical error

F = functions defined in Eq. (10)

G = Green's function

H = cascade spacing or pitch

h = spacing between two flat plates

N = total number of panel

$\vec{n}$ = surface normal

p = field point or local static pressure

q = running index over surface integration

$\vec{R}$ = distance vector in (x,y) coordinate

$\vec{r}$ = distance vector in (ξ,η) coordinate

S = panel length

NOMENCLATURE (continued)

t = time

U = reference velocity

$\vec{V}$ = total velocity

$\vec{V}_B$ = surface moving velocity

$\vec{V}_\infty$ = onset flow velocity

$\vec{v}$ = disturbance velocity

$\vec{v}_\infty$ = incoming flow velocity

W = vortex-sheet surface in the wake

x,y = global ground-fixed coordinate

α = angles defined in Eq. (10) or angle of attack

Γ = circulation around an airfoil

γ = vortex strength

Θ = blade stagger angle

κ = ratio of panel lengths

Λ = boundary surfaces

λ = a constant defined in Eq. (10)

ξ,η = local panel coordinate

ρ = fluid density

σ = source strength

Φ = total scalar velocity potential

ϕ = disturbance velocity potential

ϕ_∞ = inflow velocity potential

ω = angular rotational speed

Sub- or Superscripts

e = exact solution

m = cascade modification

s = tangent to the surface

sa = single airfoil

u = upper surface

v = vortex

ℓ = lower surface

ABSTRACT

A time-accurate potential-flow calculation method has been developed for unsteady incompressible flows through two-dimensional multi-blade-row linear cascades. The method represents the boundary surfaces by distributing piecewise linear-vortex and constant-source singularities on discrete panels. A local coordinate is assigned to each independently moving object. Blade-shed vorticity is traced at each time step. The unsteady Kutta condition applied is nonlinear and requires zero blade trailing-edge loading at each time. Its influence on the solutions depends on the blade trailing-edge shapes.

Steady biplane and cascade solutions are presented and compared to exact solutions and experimental data. Unsteady solutions are validated with the Wagner function for an airfoil moving impulsively from rest and the Theodorsen function for an oscillating airfoil. The shed vortex motion and its interaction with blades are calculated and compared to an analytic solution. For multi-blade-row cascade, the potential effect between blade rows is predicted using steady and quasi unsteady calculations. The accuracy of the predictions is demonstrated using experimental results for a one-stage turbine stator-rotor.

ADMINISTRATIVE INFORMATION

This work was supported by the Independent Exploratory Development Program, DN 509501 Element 62936N, and the Submarine Auxiliary Systems Exploratory Development Project, Program Element 62323N, Block ND3A, Project RB23P11, administrated at the David Taylor Research Center.

INTRODUCTION

Unsteady flow analyses for turbomachinery can be categorized as linear or nonlinear. The linear method uses either the linear potential approach (Verdon and Caspar, 1984) or the linear Euler approach (Hall and Crawley, 1987). The nonlinear method includes both

the nonlinear Euler and the Reynolds averaged Navier-Stokes (Rai, 1987 and Giles, 1988) methods. Linear methods use the isentropic and irrotational assumptions. Quandt (1989) has shown that the solution obtained from the unsteady linear potential-flow method gives correct fluid enthalpy, pressure, and velocity changes obtained from the traditional nonlinear Euler turbomachine energy equation. The disadvantage of using the linear potential analysis is that the method does not allow for incoming vorticity. Engineering experience (Lee et al., 1990) shows that linear potential methods are the simplest models which give accurate predictions of the very large changes in lift and moment for shock-free subsonic flows. Computational efforts increase sharply when Reynolds averaged Navier-Stokes methods are used. However, more complete physics of fluid flow, e.g. flow separation, nonlinear vortex interaction and turbulence, can be predicted. Due to the greater completeness of the nonlinear methods, these methods can be used to supplement the simplified linear approaches during a design process when experimental data are not available.

In this report, a time-accurate 2-D linear potential-flow calculation method is developed. Viscosity effects are partially accounted for in the analysis by using a nonlinear Kutta condition at the airfoil trailing edge. In applying the Kutta condition, the wake of the airfoil is represented by discrete vortices (Kim and Mook, 1986 and Yao et al., 1989). The method developed is capable of providing flow predictions for various combinations of steady and unsteady body motions. The emphasis of the present paper is on cascade flows, particularly unsteady cascade flows. Although the numerical method developed is general, cascade flows require special analyses. When calculating unsteady flows between two blade rows, the vortex/blade interaction requires detailed treatment. The unsteady cascade

predictions are possible only when the building blocks of steady cascade flow calculations and some basic unsteady single airfoil calculations are predicted correctly. This report compares calculated results for single airfoils and cascades under similar conditions. It concludes with a quasi unsteady solution for a two-blade-row cascade (Dring et al., 1982).

MATHEMATICAL MODEL

Consider a 2-D system configuration consisting of multiple airfoils and/or nonlifting bodies, or a linear multi-blade-row cascade which execute arbitrary relative motions between airfoils/bodies or between cascades in an incompressible potential flow. Let the surface of the solid boundaries be denoted by $\Lambda(\vec{R},t)$, where $\vec{R}$ is a distance vector in a global ground-fixed coordinate system (x,y) and t is time. The shear layer next to the surface Λ and the shed vorticity in the wake are assumed to consist of thin layers modelled as vortex sheets. The vortex sheets in the wake are symbolized by $W(\vec{R},t)$. They are allowed to move with the local fluid particles. The flow field can be represented by a total scalar velocity potential Φ as follows,

$$\vec{V} = \nabla\Phi = \nabla\phi_\infty + \nabla\phi = \vec{v}_\infty + \vec{v} , \qquad (1)$$

where ϕ_∞ and $\vec{v}_\infty$ represent the inflow velocity potential and velocity at infinity, including any incoming onset flow and induced flow due to a near-field disturbance. ϕ and $\vec{v}$ represent the disturbance velocity potential and velocity due to airfoils/bodies and the wake vorticity. Both the total and disturbance velocity potentials satisfy Laplace's equation

$$\nabla^2\Phi = \nabla^2\phi = 0 \,. \tag{2}$$

The problem posed is to find the velocity potential ϕ and the free wake vortex structure. To ensure a unique solution to the problem, the disturbance velocity potential is subjected to: (1) a kinematical condition applied at the surface Λ where fluid particles maintain the same normal velocity as the moving surface; (2) the Kutta-Joukowski condition of equal pressure between the upper and lower airfoil surfaces applied at the trailing edge; (3) total circulation is conserved at any time, i.e. Kelvin's theorem; and (4) a dynamical condition of continuous pressure applied at free wake vortex sheets.

Using the classical Green's function approach and Morino's formulation (Morino and Tseng, 1978) in the global coordinate system, Eqs. (1) and (2) are transformed into an integral equation

$$\begin{aligned}\phi(p) = & \frac{1}{2\pi}\int_W \phi_W(q)\frac{\partial G(p,q)}{\partial n_W}ds_q \\ & + \frac{1}{2\pi}\int_\Lambda [\phi(q)\frac{\partial G(p,q)}{\partial n} - G(p,q)\frac{\partial \phi(q)}{\partial n}]ds_q \,.\end{aligned} \tag{3}$$

Here p represents the field point on Λ while q is the running index over all panels. The symbol ϕ_W represents the velocity potential due to shed wake vortices and $\vec{n} = n_x \vec{i} + n_y \vec{j}$ and $\vec{n}_W$ are the unit outward surface normal vectors to Λ and the upper side of W. The Green's function is given by $G=\ell n(1/r)$, where r is the distance between p and q. This formulation allows $|\vec{v}(p)|$ to be equal to the vortex sheet strength $\gamma(p)$ on Λ. $\partial\phi/\partial n$ is given from the normal boundary condition

$$\nabla\Phi\cdot\vec{n} = \vec{V}_B\cdot\vec{n} \tag{4a}$$

or

$$\frac{\partial\phi}{\partial n} = \vec{V}_B\cdot\vec{n} - \frac{\partial\phi_\infty}{\partial n}, \tag{4b}$$

where $\vec{V}_B$ is the velocity, including translational and rotational speeds, of the surface Λ. For a finite number of airfoils/bodies, $\partial\phi_\infty/\partial n$ is prescribed as an onset flow $\vec{V}_o$. Equation (3) is a Fredholm integral equation of the second kind for the unknown ϕ.

The calculation of unsteady force and moment on each moving body/airfoil is reduced to an integration using the unsteady Bernoulli's equation in the global coordinate system as

$$\frac{\partial\Phi}{\partial t} + \frac{V^2}{2} + \frac{p}{\rho} = \frac{p_\infty}{\rho} + \frac{V_o^2}{2} . \tag{5}$$

Equation (5) can also be nondimensionalized by a reference velocity U. If one uses the original symbols for nondimensional variables, the following formula in a body-fixed coordinate is obtained

$$C_p = \frac{p-p_\infty}{\rho U^2/2} = -2\,\frac{\partial\phi}{\partial t} - \vec{V}\cdot(2\vec{V}_B + \vec{V}) + V_o^2 . \tag{6}$$

Here the velocity potential of the onset flow is assumed to be steady.

NUMERICAL METHOD

Singularity Distributions

The surface Λ is discretized into small line segments. The control point for each segment is located at the center of the segment. The normal to the surface is approximated by the perpendicular to the straight segment. The distributions of the vortices and the sources on each segment are assumed to be linear and constant, respectively. The velocity potential at a field point p due to a line segment q of length S with a constant unit-strength source, i.e. $\sigma(\xi)=1$, in a local line-segment coordinate (ξ,η) as shown in Fig. 1 is

$$\begin{aligned} 2\pi\phi_o(p,q) &= \int_{-\frac{S}{2}}^{\frac{S}{2}} \sigma(\xi)\,\ln\frac{1}{r(p,\xi)}d\xi \\ &= S-\eta_p F_1-\xi_p F_3-\frac{S}{2}F_4 \ . \end{aligned} \tag{7}$$

The velocity potential at the point p due to a constant unit-strength vortex, i.e. $\gamma(\xi)=1$, is

$$\begin{aligned} 2\pi\phi_{\gamma U}(p,q) &= \int_{-\frac{S}{2}}^{\frac{S}{2}} \gamma(\xi)\,\arctan\frac{\xi-\xi_p}{\eta_p}d\xi \\ &= \frac{\xi_p}{2}F_1-F_2-\frac{\eta}{4}F_3 \ . \end{aligned} \tag{8}$$

The velocity potential corresponding to a linearly distributed vortex sheet, i.e. $\gamma(\xi)=2\xi/S$, is

$$\begin{aligned} 2\pi\phi_{\gamma L}(p,q) &= \int_{-\frac{S}{2}}^{\frac{S}{2}} \gamma(\xi)\,\arctan\frac{\xi-\xi_p}{\eta_p}d\xi \\ &= \frac{\eta_p}{2}+\frac{1}{2S}(\xi_p^2-\eta_p^2-\frac{S^2}{4})F_1-\frac{1}{2S}\xi_p\eta_p F_3 \ . \end{aligned} \tag{9}$$

In Eqs. (7)-(9) we have

$$
\begin{aligned}
F_1 &= \alpha_1-\alpha_2 \\
F_2 &= \pi-\alpha_1-\alpha_2+2\pi\lambda \\
F_3 &= \ln(R_1/R_2) \\
F_4 &= \ln(R_1R_2) \\
R_1 &= [(\frac{S}{2}+\xi_p)^2+\eta_p^2]^{1/2} \\
R_2 &= [(\frac{S}{2}-\xi_p)^2+\eta_p^2]^{1/2} \\
\alpha_1 &= \arctan\frac{\xi_p+S/2}{\eta_p} \\
\alpha_2 &= \arctan\frac{\xi_p-S/2}{\eta_p} \ .
\end{aligned}
\tag{10}
$$

The function F_2 is multiple valued when $\xi_p>0$ and $|\eta_p|$ approaches zero, i.e. $\lambda=1$ when η_p crosses the positive real axis from positive η_p, $\lambda=-1$ when η_p crosses the positive real axis from negative η_p, and $\lambda=0$ for all other cases. Thus the velocity potential at an ith segment due to a jth segment which contains uniformly and linearly distributed vortices, i.e. $\gamma(\xi)=(\gamma_j+\gamma_{j+1})/2+(\gamma_{j+1}-\gamma_j)\xi/2S_j$ as shown in Fig. 2, and a constant source is given by

$$
\phi_{ij} = CDI_{ij}\gamma_j+CD2_{ij}\gamma_{j+1}+CS_{ij}\sigma_j \ , \tag{11}
$$

where

$$
\begin{aligned}
CDI_{ij} &= \frac{1}{2}(CDU_{ij}-CDL_{ij}) \\
CD2_{ij} &= \frac{1}{2}(CDU_{ij}+CDL_{ij}) \ ,
\end{aligned}
\tag{12}
$$

and CDU_{ij} and CDL_{ij} represent the velocity potentials due to the uniformly and the linearly distributed vortices from Eqs. (8) and (9), and CS_{ij} is due to the uniformly distributed source from Eq. (7). The velocity potential at p due to a discrete shed vortex in the wake is

$$2\pi\phi_W(p,q) = \gamma_W(q) \arctan\frac{y_p - y_q}{x_p - x_q} . \tag{13}$$

Matrix Equation for Bound Vortex γ

For a unique solution outside of the surface Λ described by Eq. (3), the flow inside the surface Λ can be assumed at rest. If each body/airfoil surface Λ is divided into N segments, the interior flow-quiescent condition requires

$$\nabla\phi = \phi_{i+1} - \phi_i = 0 \qquad i=1,2...,N-1 . \tag{14}$$

The no-penetration boundary condition, Eq. (4), is imposed at the control point of each line segment. By substituting Eqs. (3), (4), (11) and (12) into Eq. (14), a set of linear algebraic equations for the bound vortex γ is formed

$$\begin{aligned}
&(CD1_{i,1} - CD1_{i-1,1})\gamma_1 + CD2_{i,N} - CD2_{i-1,N})\gamma_{N+1} \\
&\quad + \sum_{j=1}^{N-1} (CD1_{ij+1} - CD1_{i-1j+1} + CD2_{ij} - CD2_{i-1j})\gamma_{j+1} \\
&= \sum_{j=1}^{N} (CS_{ij} - CS_{i-1j})\frac{\partial\phi}{\partial n_j} - \sum_{j=1}^{ITS-1} \gamma_{Wj}\phi_{Wj} \\
&\qquad\qquad i=1,2....,N-1 .
\end{aligned} \tag{15}$$

Here ITS represents the total time steps. Equation (15) forms N-1 equations for N+1 unknown values of γ. Hence two extra equations are required for obtaining a unique solution.

Extra Conditions for Nonlifting Body

An unsteady potential flow past a nonlifting body generally does not shed vorticity in

the wake. Hence an extra condition can be obtained by requiring

$$\gamma_1 = \gamma_{N+1} \tag{16}$$

for a closed body, where γ_1 and γ_{N+1} are the first and the last vortex strengths as defined in Eq. (15). Since no lift will be generated, a zero net circulation around the body can be used, i.e.

$$\sum_{j=1}^{N} S_j(\gamma_j+\gamma_{j+1}) = 0 \ . \tag{17}$$

Equations (15), (16) and (17) form a set of linear equations for determining γ on a non-lifting configuration.

Nonlinear Kutta Condition for Lifting Body

The Kutta-Joukowski condition was originally applied to two-dimensional steady flow in order to obtain a finite velocity at the trailing edge, and as a consequence, the flow is uniquely determined. This hypothesis implicitly accounts for viscous effects otherwise neglected in the potential-flow theory. Instead of requiring a velocity condition at the trailing edge, a pressure condition is used in the present numerical model. Since the trailing edge does not account for any loading, the pressures there on the upper surface (sub- or superscript u) and the lower surface (sub- or superscript ℓ) are required to be the same. It is worth noting that this condition does not refrain the trailing edge from having a variation of pressure in the time domain. Using Eq. (6), one obtains

$$2\frac{\partial}{\partial t}(\phi_u-\phi_\ell)+[(\vec{V}+\vec{V}_B)_u\cdot(\vec{V}+\vec{V}_B)_u - (\vec{V}+\vec{V}_B)_\ell\cdot(\vec{V}+\vec{V}_B)_\ell] = 0 . \tag{18}$$

Since the impermeable boundary condition is applied at Λ, the flow on the upper and lower surfaces is along the tangents (sub- or superscript s) to both surfaces. Use Eq. (1) and the following relations

$$\phi_u-\phi_\ell \equiv \Gamma = \sum_{j=1}^{N}\frac{1}{2}(\gamma_j+\gamma_{j+1})S_j$$
$$\bar{v}_t \equiv \frac{1}{2}(v_\infty^{su}-v_\infty^{st}+v^{su}-v^{st}+V_B^{su}-V_B^{st}) , \tag{19}$$

Eq. (18) is cast as

$$(1+\frac{S_1}{2VT})\gamma_1+\sum_{j=1}^{N-1}\frac{S_j+S_{j+1}}{2VT}\gamma_{j+1}+(1+\frac{S_N}{2VT})\gamma_{N+1} = \frac{-\Gamma(t-\Delta t)}{VT}-v_\infty^{su}-v_\infty^{st} . \tag{20}$$

where $VT = 2(\Delta t)\bar{v}_t$ and Γ is the circulation of the airfoil and defined as positive in a clockwise direction. Equation (20) is linear in γ if VT is considered to be a constant. In the present study, Eq. (20) is solved iteratively to account for the nonlinearity of VT. Both Yao et al. (1989) and Kim and Mook (1986) applied a more restricted Kutta condition at the trailing edge by requiring $\gamma_1=\gamma_{N+1}=0$ and placing a wake vortex of unknown strength there. This implies that their algebraic equations are linear and require an optimization technique to produce a deterministic system.

For the present scheme, according to Eq. (15) one more equation is needed in order to obtain a unique γ-distribution for a lifting body. This condition is provided by requiring

the velocity gradients along the tangents at the trailing edge from both the upper and lower surfaces to be the same, i.e.

$$(\frac{\partial \gamma}{\partial s})_u = (\frac{\partial \gamma}{\partial s})_l \ . \tag{21}$$

Allowing the equality of velocity gradients from the upper and the lower surfaces at the trailing edge further ensures the smooth merge of two jet flows. Experience also indicates that this condition offers stable and accurate predictions. When a second-order backward differencing scheme is used, Eq. (21) is transformed to

$$\gamma_{N+1} = \frac{\kappa[\kappa_l(2+\kappa_l)\gamma_1 - (1+\kappa_l)^2\gamma_2 + \gamma_3] + (1+\kappa_u)^2\gamma_N - \gamma_{N-1}}{\kappa_u(2+\kappa_u)} \tag{22}$$

where $\kappa_u = S_{N-1}/S_N$, $\kappa_l = S_2/S_1$ and $\kappa = S_{N-1}(1+\kappa_u)/S_2(1+\kappa_l)$. Hence Eqs. (15), (20) and (22) form a determinate system of nonlinear equations for determining γ for a lifting configuration. They are solved using an iterative scheme.

Determination of Shed Vorticity

Kelvin's theorem states that the total circulation of the fluid at any instant is conserved. This condition provides a mechanism to shed vorticity into the wake. At each time step, a uniformly distributed vortex segment with strength γ_W is generated in the wake adjacent to the airfoil trailing edge. The length S_W of the vortex segment is the distance the trailing edge moves between t-Δt and t. At a subsequent time step this uniform line vortex is replaced by a discrete concentrated vorticity of equivalent strength located at the center of

the segment. The generated trailing-edge vortex segment relates to the airfoil circulation Γ as follows

$$\frac{\Gamma(t)-\Gamma(t-\Delta t)}{\Delta t}+\frac{S_W(t)\gamma_W(t)}{\Delta t} = 0 \ . \tag{23}$$

The model depicted in Eq. (23) yields stable solutions which are independent of the time-step used. However, for the present calculations the solutions were found to be dependent on the time step used if a concentrated vorticity model was adopted for modeling the trailing-edge vortex generation. The latter model was used in Kim and Mook's model (1986). Since the time step used by Kim and Mook was extremely small, they may not be aware of the time dependency of the discrete vortex generating mechanism at the trailing edge.

The wake vortices are convected downstream and develop a vorticity field. In the present numerical scheme, these vortices are tracked through the flow field using Lagrangian techniques. The convection of these discrete vortices is modelled by a predictor-corrector scheme as

$$\vec{r}_W^{(1)}(t+\Delta t) = \vec{r}_W(t)+\vec{v}_W[\vec{r}_W(t),t]\Delta t \tag{24a}$$

$$\vec{r}_W^{(2)}(t+\Delta t) = \vec{r}_W^{(1)}(t+\Delta t) + \frac{1}{2}\left(\vec{v}_W[\vec{r}_W^{(1)}(t+\Delta t),t]-\vec{v}_W[\vec{r}_W(t),t] \right)\Delta t \tag{24b}$$

$$\vec{r}_W(t+\Delta t) = \vec{r}_w^{(2)}(t+\Delta t) \ . \tag{24c}$$

The superscripts in parentheses represent the iteration number within each time step. The corrector in Eq. (24b) is particularly important for a body oscillating at low frequency. For

such a flow, $\partial\Gamma/\partial t$ is relatively small in Eqs. (18) and (19). Both equations imply that the nonlinear effect in the Kutta condition is strong and the velocity prediction within each time step plays a dominant role in obtaining a converged solution. Giesing (1969) also used a predictor-corrector scheme to convect the vortices in the wake, but treated the intermediate iteration step as a complete separate "time step". The present calculation only uses the corrector to locate the new vortex positions without performing the rest of the calculations at the next time step. Hence the calculation time only increases slightly. Kim and Mook (1986) used only Eq. (24a) for vortex convection, but their time step is rather small.

Special Considerations for a Cascade

For a cascade of blades with pitch H, each blade generates a circulation. If the cascade runs along the y-axis, there exists an upwash at upstream infinity of the cascade and a downwash at downstream infinity. In conjunction with a specified inflow onset condition as shown in Eq. (4), an extra term is needed to ensure a unique upstream inflow condition, i.e.

$$\frac{\partial \phi_\infty}{\partial n} = n_y \sum_{mj=1}^{MJ} \frac{\Gamma_{mj}}{2H_{mj}} \tag{25}$$

for a multi-blade-row cascade flow, where MJ is the total number of blade rows, H_{mj} is the mj-th cascade spacing or pitch, and Γ_{mj} is the blade circulation from the mj-th cascade.

In a cascade configuration, the velocity potentials at a field point p due to a point source and a point vortex on a blade surface q can be written as

$$\phi_\sigma(p,q) = -\frac{1}{2\pi}\ln[\sinh^2\bar{H}(x_p-x_q)\cos^2\bar{H}(y_p-y_q) + \cosh^2\bar{H}(x_p-x_q)\sin^2\bar{H}(y_p-y_q)]^{1/2} \quad (26a)$$

$$\phi_\gamma(p,q) = \frac{1}{2\pi}\arctan\frac{\sin\bar{H}(y_p-y_q)}{\sinh\bar{H}(x_p-x_q)}, \quad (26b)$$

where $\bar{H}=\pi/H$. Equation (11) is therefore modified to

$$\begin{aligned}\phi_i &= \sum_j(\sigma_j\phi_{\sigma ij}+\gamma_j\phi_{\gamma ij}) \\ &= \sum_j(\sigma_j\phi^{sa}_{\sigma ij}+\gamma_j\phi^{sa}_{\gamma ij})+\sum_j[\sigma_j(\phi_{\sigma ij}-\phi^{sa}_{\sigma ij})+\gamma_j(\phi_{\gamma ij}-\phi^{sa}_{\gamma ij}) \\ &= \phi_i^{sa}+\phi_i^{m}\end{aligned} \quad (27)$$

where superscripts sa and m represent the corresponding single airfoil and its cascade modification. ϕ^{sa}'s are defined as

$$\phi^{sa}_{\sigma ij} = -\frac{1}{2\pi}\ln\sqrt{x_i^2+y_i^2} \quad (28a)$$

$$\phi^{sa}_{\gamma ij} = \frac{1}{2\pi}\arctan\frac{y_i}{x_i}, \quad (28b)$$

and the cascade modification is

$$\phi_{\sigma ij}-\phi^{sa}_{\sigma ij} = -\frac{1}{2\pi}\ln[\frac{\sinh^2\bar{H}x_i+\sin^2\bar{H}y_i}{(\bar{H}x_i)^2+(\bar{H}y_i)^2}]^{1/2} \quad (29a)$$

$$\phi_{\gamma ij}-\phi^{sa}_{\gamma ij} = \frac{1}{2\pi}\arctan\frac{x_i\sin\bar{H}y_i-y_i\sinh\bar{H}x_i}{x_i\sinh\bar{H}x_i+y_i\sin\bar{H}y_i}. \quad (29b)$$

A complete integration of the velocity potentials for the source and the vortex distributions on each segment was performed numerically for the cascade modification term ϕ_i^m in Eq. (27).

APPLICATIONS

The present calculation method was first validated by comparison to known steady flows. Steady-flow comparisons are presented for two cases. The first case is for flow past a biplane, which has an exact conformal mapping solution (Robinson and Laurmann, 1956). The second steady flow calculation is for flows past a NACA65-1210 cascade for which the solutions compared to measured values (Herrig et al., 1957). For unsteady flows, four cases calculated using the present method are presented. They include the following three basic blade motions: an airfoil moving impulsively from rest, an oscillating airfoil, and a vortex interacting with an airfoil. Calculations were made for both a single airfoil and a cascade under each of the specified blade motions. The last case presented is a quasi-unsteady calculation for a two-blade-row stator-rotor configuration.

Steady Flows

The main purpose of investigating flows past a biplane, i.e. two flat plates, is threefold: to examine the accuracy of the prediction when compared to an exact solution; to numerically explore the limits of the prediction scheme; and to understand the prediction capability of the nonlinear Kutta condition.

Figure 3d shows a schematic of the biplane geometry and inflow description. The comparisons between the present calculated results and the exact conformal mapping solutions in Fig. 3a correspond to a constant inflow angle $\alpha = 20^{\circ}$, and various spacings between two plates. When the spacing is large, pressure distributions are identical on the two plates. As the spacing is reduced, a stronger interaction between the two plates is

observed. The pressure of the lower surface of the upper plate approaches that of the upper surface of the lower plate. Figures 3b and 3c show the effect of varying the inflow angle under the condition of strong plate interaction. As α varies from 20° to 90°, the pressure on the lower surface of the upper plate stays nearly the same as that on the upper surface of the lower plate. However, the lift generated by the lower plate is reduced as α increases. The zero-lift α for the lower plate at h/c=0.228 is between 50° and 65°. For α larger than the zero-lift value, the lower plate actually begins to generate negative lift. When α approaches 90° as shown in Fig. 3c, the pressure curve for the upper surface of the upper plate matches that for the lower surface of the lower plate, and similarly for the other surfaces of both plates. The total lift of the two-plate system is zero. When the spacing between the two plates increases at α =90°, the pressures on the lower surface of the upper plate and on the upper surface of the lower plate approach those of the other surfaces. At h/c=9.708 as shown in Fig. 3c, the pressures on all the surfaces coincide and the interaction between the two plates is minimum. Although in reality flow separates at high values of α, the present numerical calculations serve the purpose of validating the implemented numerical procedures under extremely severe flow conditions by comparing with the conformal-mapping solutions. For all the cases predicted, the present results agree well with the exact solutions and show extremely "clean" predictions at both the leading and the trailing edges.

Steady flows through a cascade of NACA65-1210 blades were also examined. Figure 4a shows the calculated blade pressure distributions compared to measurements (Herrig et al., 1957) at two different inlet flow angles (α_1 = 12.1° and 16.1°) and blade stagger

angles (Θ=-32.9° and -28.9°). Flow is at the design condition for the first case. The predicted blade loading agrees well with the measurements. The computed blade-to-blade pressure contours for flows past a single airfoil and a cascade are depicted in Figure 4b. The results indicate that the pressure gradients for the cascade due to blockage is larger than that of the single foil, particularly in the leading and trailing edge areas. The computed flow turning angles through the cascade for both cases are 21.98° and 26.13° versus the measured values of 19.6° and 23.3°. If an estimated boundary-layer displacement thickness of 0.4% of the chord, obtained based on a flat-plate boundary layer, at the trailing edge is added to the airfoil ordinates, the calculated turning angles become 19.99° and 23.8°. This modification in the calculation procedure indicates that the cascade exit flow angle depends also on the viscous effect in the trailing-edge area.

The numerical error E of the present calculations was evaluated based on

$$E = \frac{1}{N}[\sum_{i=1}^{N}(C_p - C_{pe})^2]^{1/2} \tag{30}$$

where C_{pe} represents the exact pressure distribution. There are two cases in Fig. 5 to show the numerical convergence versus the panel numbers used. The first case shown in Fig. 5a is for nonlifting flows past a circular cylinder. The panel numbers used range from 20 to 600. The second case shown in Fig. 5b is for lifting flows past either a single NACA 0010 airfoil or two NACA 0010 airfoils. The exact pressure distributions used for calculating errors are the numerical solutions of 1000 panels for the single airfoil and 500 panels for the bifoil. The numerical convergence rate shown in Fig. 5b is independent of the number of the airfoils, but it decreases as the angle of attack increases. Since the coarse grid points do

not usually match with the finest grid points used as the exact solution, the convergence dependency on the angle of attack relates to the inaccurate interpolated exact C_p-distribution in the leading-edge area when the slope becomes steep for large angles of attack. Nevertheless, based on this analysis using 100 panels for a closed body indicates that the error of the solution is under 10^{-4}.

Unsteady Flows

Figure 6a shows the calculated transient lift coefficients as a function of the airfoil traveling distance for an impulsively moving NACA 0012 airfoil of 4% thickness at an angle of attack of 5° and two cascades with different spacings (H) as compared to the exact Wagner function (Fung, 1969) for a single airfoil. The wake pattern of the calculated single airfoil case is depicted in Fig. 6b. Figure 6c shows the calculated vortex locations for the three cases. The results indicate that the length of the transient phenomenon becomes shorter for the cascade flow.

Figure 7 shows a similar comparison for oscillating NACA 0012 blades. The exact solution plotted is the Theodorsen function (Fung, 1969) at a reduced frequency $\omega c/U$ of 17. The time step chosen is to cover one period of the oscillating motion with minimum 25 points. The amplitude of the calculated lift coefficients using the present method, referring to $(C_L)_T$ versus $\tau(=\omega t)$ in Fig. 7a, is smaller for the cascade data. The shed vortex patterns, shown in Fig. 7c, of the single foil and the cascades are compared to the flow visualization of Bratt (1950), shown in Fig. 7b, for a single NACA 0015 airfoil. The width of the cascade vortex wakes in Fig. 7c is predicted to be slightly smaller than that of the single foil. This

result demonstrates that the cascade effect is more important than the wake vortex structure for predicting the blade loading.

Figure 8c shows the time history of the shed vortices for a NACA 0012 section at zero angle of attack interacting with an incoming vortex initially located upstream of the airfoil at $y_v/c=-0.13$. The calculated instantaneous lifts versus vortex locations (the airfoil is located between 0 and 1) for the single foil are shown in Fig. 8a as compared with Lee and Smith's (1987) solutions . The lift decreases first to a negative value, recovers quickly to a positive value, and drops slowly to near zero when the vortex passes through the airfoil. Two curves for different vertical separation distances between the airfoil and the vortex are depicted. When the vortex is placed closer to the airfoil, the effect of producing a fluctuating lift is more pronounced. Figure 8b shows the calculated lifts for both single foils and cascades. For the cascade results, the fluctuation in lifts when the vortex passing through the leading edge and the trailing edge of the airfoil is suppressed significantly. This may suggest that vortical flows through turbomachinery blade passages are distributed in a more orderly fashion than one might expect based on a single airfoil motion.

Figure 9 presents calculated 2D quasi unsteady two-blade-row cascade results and corresponding 3D measurements (Dring et al., 1982). The turbine consists of a 22-blade stator with pitch $H=0.854c$ and a 28-blade rotor with pitch $H=0.813c$. Both the stator and the rotor have round trailing edges. The gap between the two blade rows is 15% of the stator chord. The calculated steady solutions under uniform flows of zero angles of attack for each separate blade row are shown in Fig. 9a. Due to the fact that the unknown inlet flow angle for the rotor blade row was specified incorrectly as an input parameter, the

pressure prediction in the rotor leading edge area does not agree with the measured data at all. The pressure prediction in the rotor trailing edge area is, however, independent of the its inlet flow angle and relates to the viscous effect and the application of the Kutta condition. Since the rotor operates at a reduced passing frequency of 2.8 (based on the turbine diameter), both the stator trailing edge and the rotor leading edge sense a variation of pressure. Figure 9b shows the "time-averaged" maximum and minimum pressure distributions of the steady calculations for both stator-rotor blade rows at 10 different relative blade locations, which represent a full cycle of the stator-rotor blade interaction. The measured values shown in the Fig. 9b are also the time-averaged pressures and the range of the unsteady fluctuating pressures (represented by the uncertainty symbols centered at the time-averaged value). The calculated quasi unsteady pressure ranges are larger at the stator trailing edge and the rotor leading edge than the measured ranges. They become smaller elsewhere. The predicted large fluctuations near the stator and the rotor trailing edges are associated with the round shapes when the Kutta condition is enforced at the centers of the trailing-edge circular arcs. Since small trailing-edge separation bubbles are expected for both the rotor and the stator, a more realistic location for applying the Kutta condition would be some point outside the circular arcs. However, this influence will be very localized. These results clearly demonstrate a strong potential effect of the stator flow on the rotor flow. It also shows the capability and accuracy of the 2D potential-flow calculations.

CONCLUSIONS

A time-dependent potential-flow method is described to calculate the vortex shedding and blade-vortex interaction for cascades and for single airfoils. Without a separation, the steady potential-flow calculation has the capability of accurately predicting the cascade blade loading. A simple inclusion of the boundary-layer displacement effect enables the present calculation to predict the cascade exit flow conditions reliably. The unsteady interaction phenomena between the incoming vortex field or the wake shedding vorticity field and the airfoil are found to be similar for the single airfoil and cascade flows. The predicted periodic blade lifts have smaller amplitude for the cascade flows. For the transient calculations, i.e. the Wagner function prediction, the cascade flow approaches steady state much faster than the single airfoil flow. The present calculation method has been shown to be effective in predicting steady and unsteady flows through a multi-blade-row cascade.

ACKNOWLEDGEMENTS

The computing time was provided by the Numerical Aerodynamic Simulation Program of the NASA Ames Research Center. The pressure distributions presented in Fig. (4a) were obtained by Alan Becnel of DTRC using the present developed computer code.

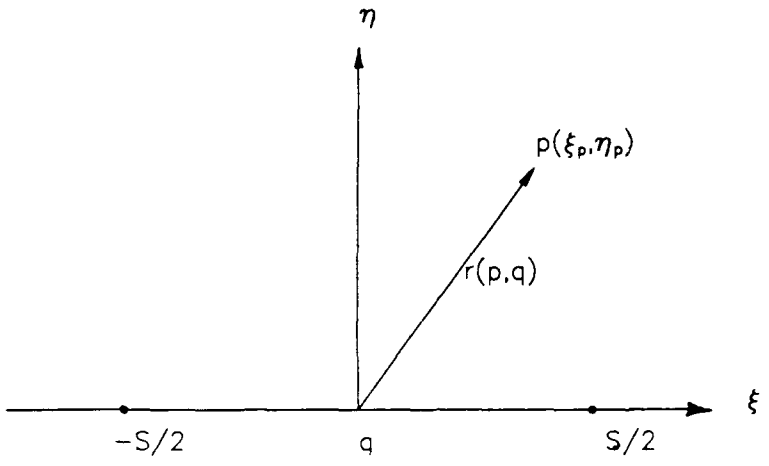

Fig. 1 Schematics for a line segment

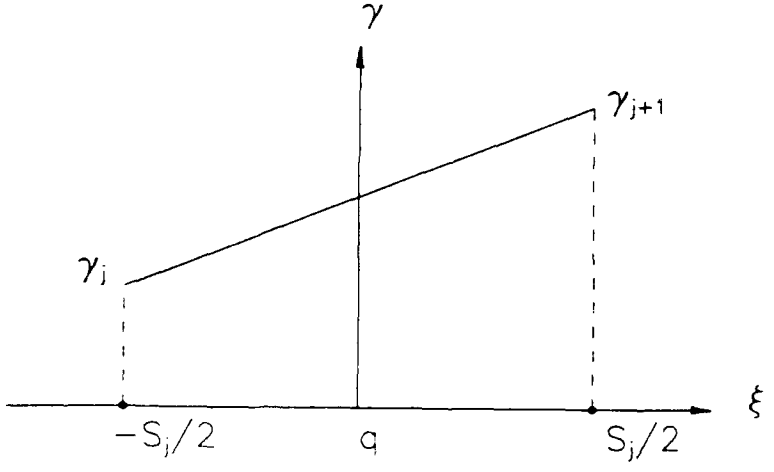

Fig.2 Linearly distributed vortex on a line segment

Plate	Conformal Mapping	Present Calculation
Upper	———	□
Lower	----------	x

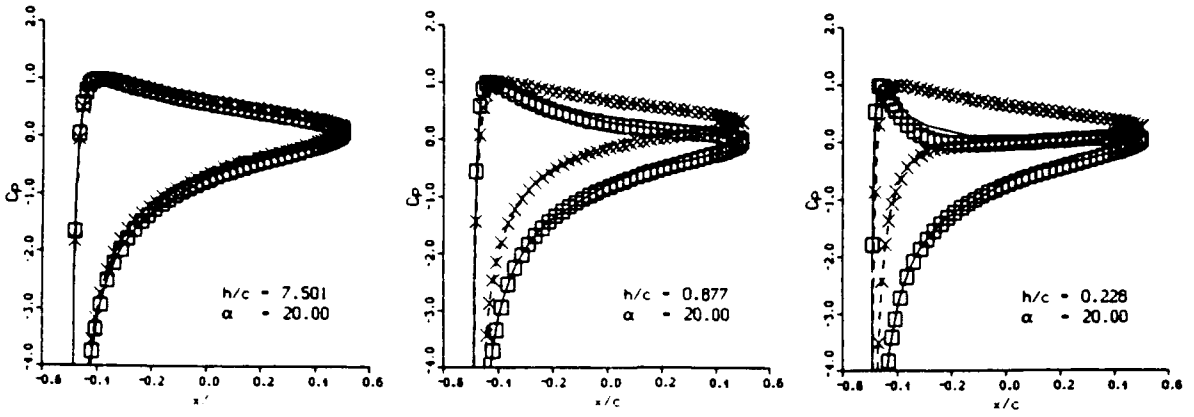

(3a) Varying plate spacing

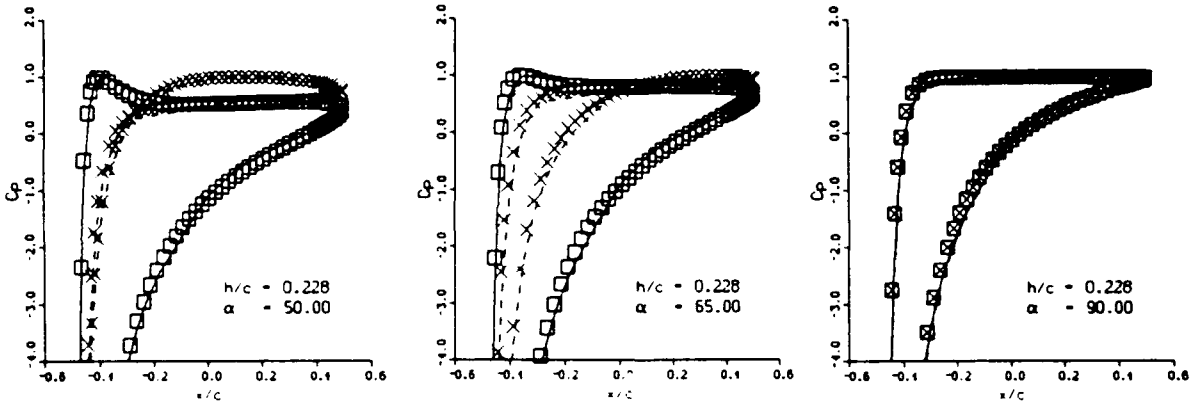

(3b) Varying inflow angle

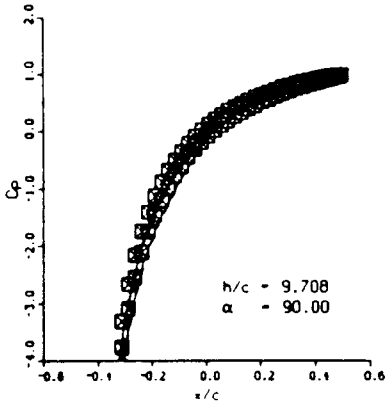

(3c) Large spacing at $\alpha = 90°$

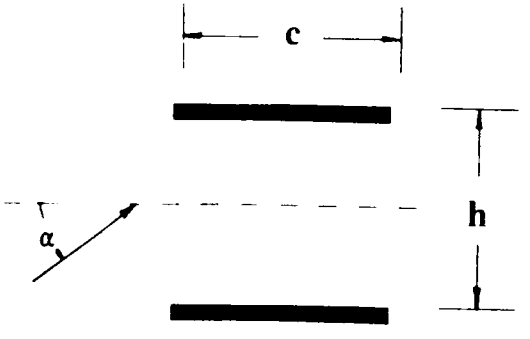

(3d) Geometry schematic

Fig.3 Pressure distributions on a biplane

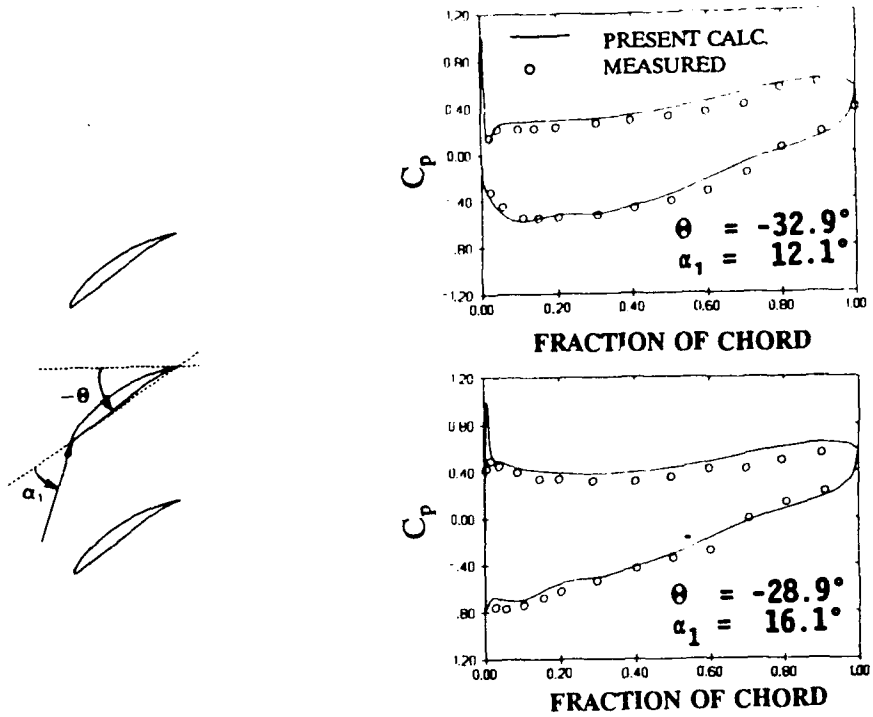

(4a) Predicted pressure distributions

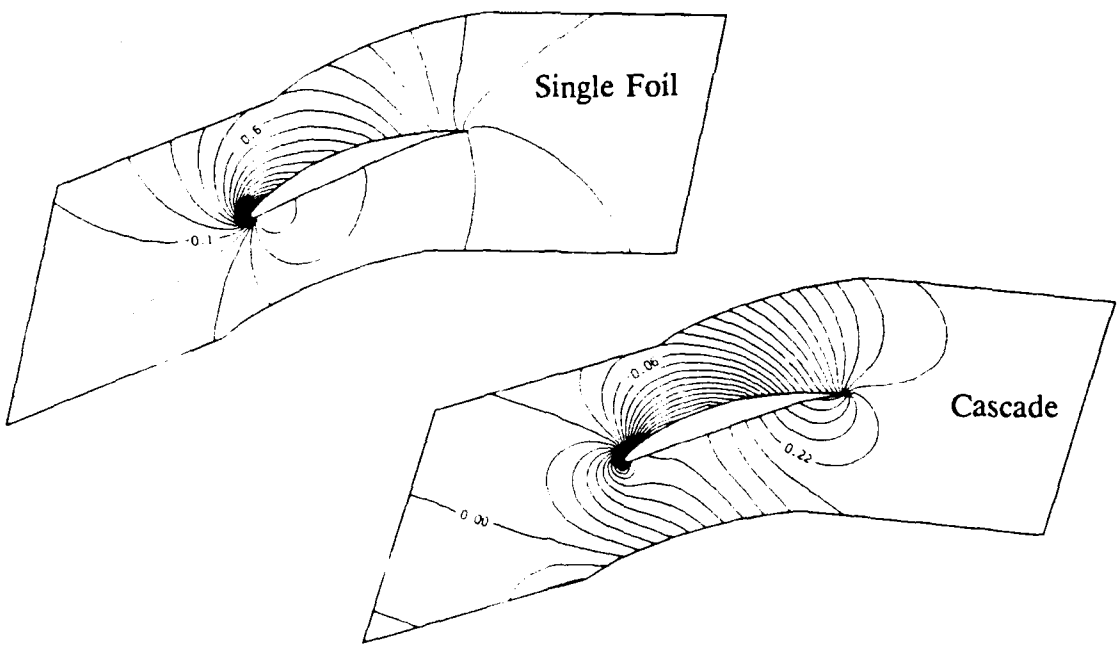

(4b) Blade-to-blade pressure contours

Fig.4 Calculation for NACA65-1210 cascade

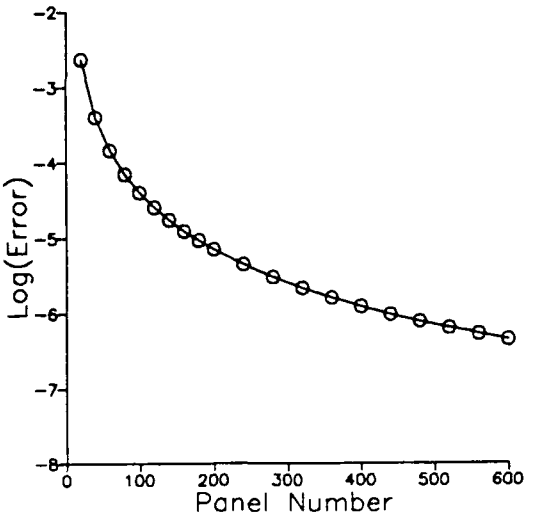

(5a) For a circular cylinder

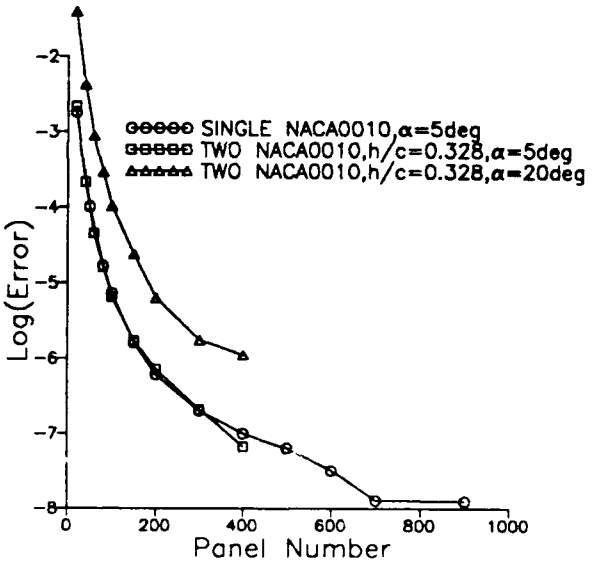

(5b) For one and two NACA 0010 airfoils

Fig.5 Numerical convergence versus panel numbers

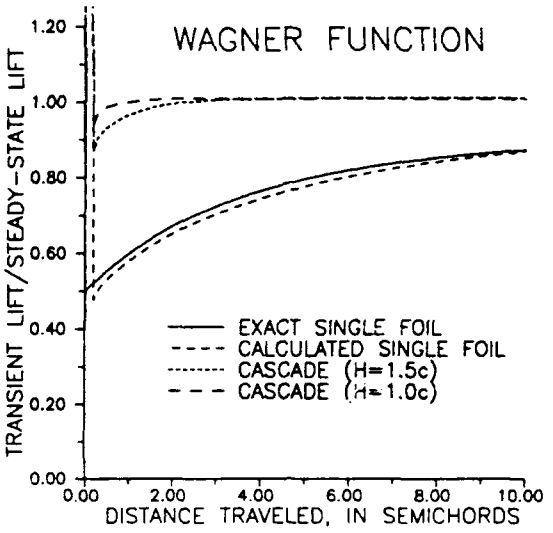

(6a) Instantaneous lift

(6b) Wake pattern for a single airfoil

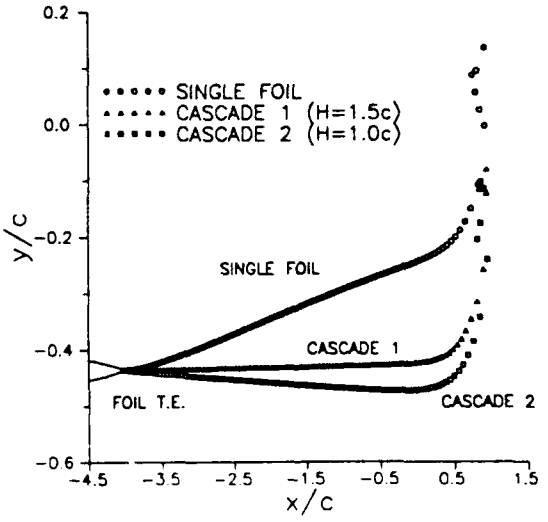

(6c) Wake vortex locations

Fig.6 Predictions for impulsively starting airfoils

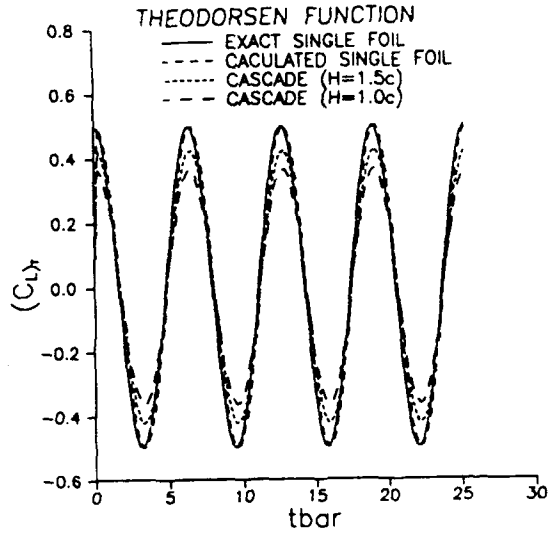

(7a) Instantaneous lift

(7b) Flow visualization of Bratt for a NACA 0015 airfoil

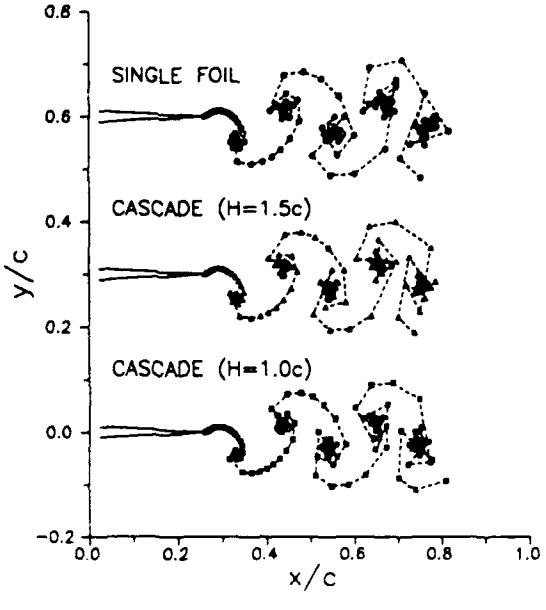

(7c) Wake vortex locations

Fig.7 Predictions for oscillating NACA 0012 airfoils at a reduced frequency of 17

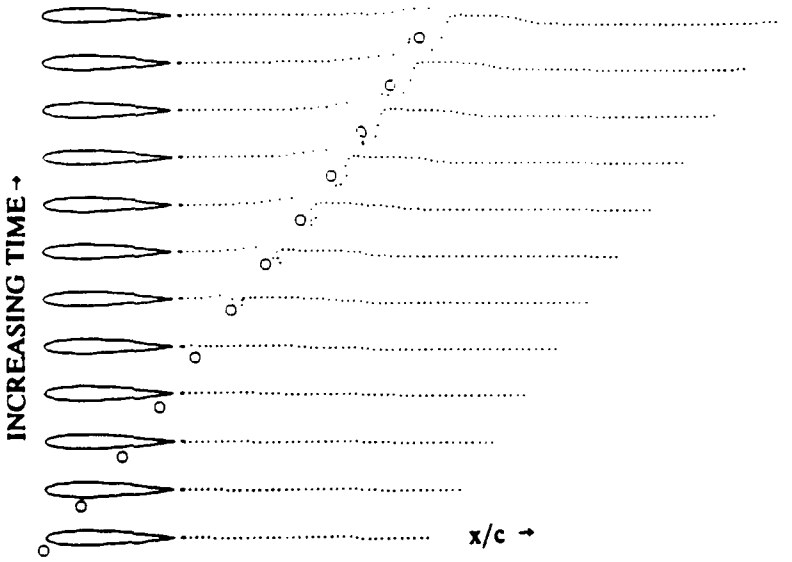

(8a) Incoming vortex at $y_v/c=-0.13$ interacts with wake vortices

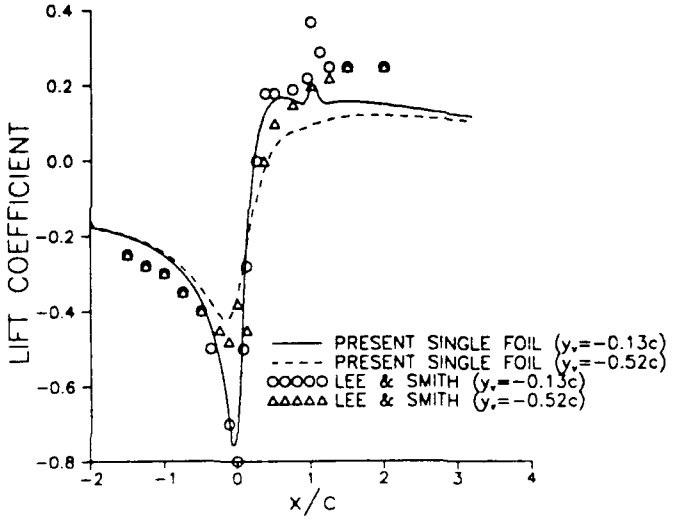

(8b) Instantaneous lift for single airfoil

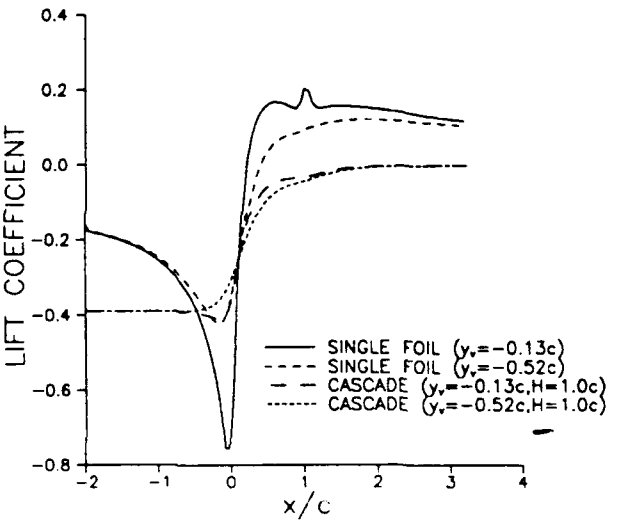

(8c) Calculated instantaneous lift for cascades

Fig.8 Incoming vortex interacting with airfoil

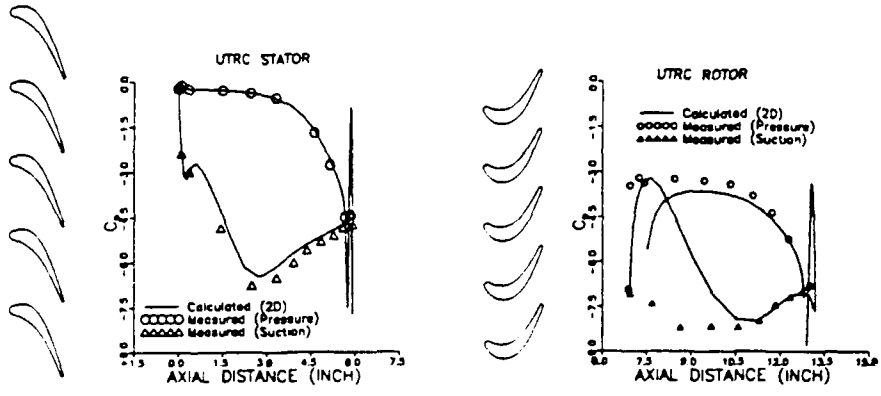

(9a) Considering stator and rotor separately under uniform flows at zero angle of attack

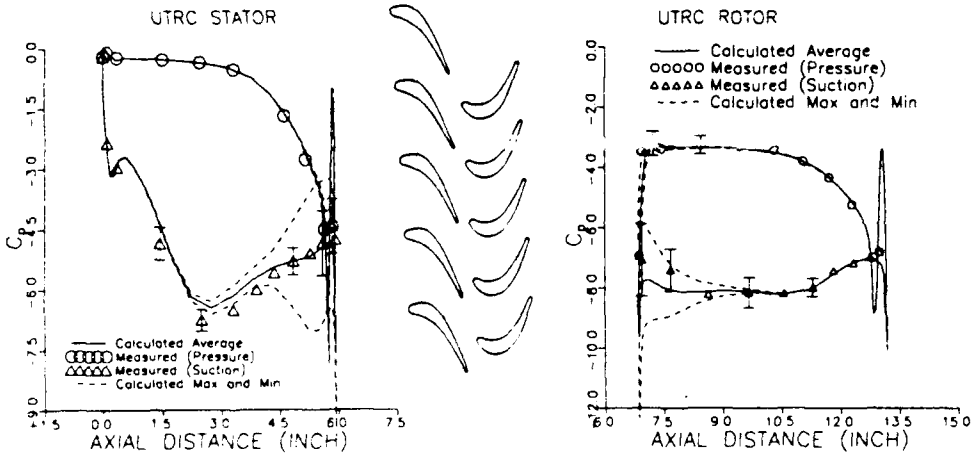

(9b) Considering stator and rotor as one single unit

Fig.9 Quasi unsteady blade-loading predictions for UTRC stator and rotor

REFERENCE

Bratt, J.B., 1950, "Patterns in the Wake of an Oscillating Aerofoil," *Royal Aeronautical Establishment*, R&M 2773, pp.269-295.

Dring, R.P., Joslyn, H.D., Hardin, L.W., and Wagner, J.H., 1982, "Turbine Rotor-Stator Interaction," *Journal of Engineering for Power*, Vol. 104, pp.729-742.

Fung, Y.C., 1950, *An Introduction to the Theory of Aeroelasticity*, Dover, New York, pp.207 & 401-407.

Giesing, J.P., 1969, "Vorticity and Kutta Condition for Unsteady Multi-Energy Flows," *Journal of Applied Mechanics*, Vol.36, Series E, pp.608-613.

Giles, M.B., 1988, "Calculation of Unsteady Wake Rotor Interaction," *AIAA J. of Propulsion and Power*, Vol. 4.

Hall, K.C., and Crawley, E.F., 1987, "Calculation of Unsteady Flows in Turbomachinery Using the Linearized Euler Equations," *Proc. of 4th Sym. on Unsteady Aerodynamics and Aeroelasticity of Turbomachines and Propellers*.

Herrig, L.J., Emery, J.C., and Erwin, J.R., 1957, "Systematic Two-Dimensional Cascade Tests of NACA 65-Series Compressor Blades at Low Speeds," NACA Technical Note 3916.

Kim, M.J., and Mook, D.T., 1986, "Application of Continuous Vorticity Panels to General Unsteady Incompressible Two-Dimensional Lifting Flows," *Journal of Aircraft*, Vol.23, No.6, pp.464-471.

Lee, D.J., and Smith, C.A., 1987, "Distortion of the Vortex Core During Blade/Vortex Interaction," AIAA Paper 87-1243.

Lee, Y.T., Jiang, C.W., and Bein, T.W., 1990, "Rotor/Stator Flow Coupling in

Turbomachines," *Proc. of 3rd Intern. Sym. on Transport Phenomena and Dynamics of Rotating Machinery*, J.H. Kim and W.-J. Yang, ed., Honolulu, Hawaii.

Morino, L., and Tseng, K., 1978, "Time-domain Green's Function Method for Three-Dimensional Nonlinear Subsonic Flows," *AIAA 11th Fluid and Plasma Dynamics Conference*, Seattle, Washington, Paper 78-1204,.

Quandt, E., 1989, "The Acoustic Radiation from Unsteady 3-D Potential Flow Vortex System Produced by Turbomachine Blade Motions," ASME Paper No. 89-WA/NCA-10.

Rai, M.M., 1987, "Unsteady Three-Dimensional Navier-Stokes Simulations of Turbine Rotor-Stator Interaction," AIAA Paper 87-2058.

Robinson, A., and Laurmann, J.A., 1956, *Wing Theory*, Cambridge at the University Press, pp.137-142.

Verdon, J.M. and Caspar, J.R., 1984, "A Linearized Unsteady Aerodynamic Analysis for Transonic Cascades," *Journal of Fluids Mechanics*, Vol. 149, pp.403-429.

Yao, Z.X., Garcia-Fogeda, P., Liu, D.D., and Shen, G., 1989, "Vortex/Wake Flow Studies For Airfoils in Unsteady Motions," AIAA Paper 89-2225.

INITIAL DISTRIBUTION

Copies	
2	CNO
1	222
1	22T
6	ONT
1	21
1	21B
1	211 (Gagorik)
1	23 (Faulstitch)
1	23B (Fitch)
1	233 (Remmers)
2	ONR
1	113
1	1215 (Fein)
14	NAVSEA
1	SEA 05R24 (Culbertson)
1	SEA 05R32 (Smookler)
1	SEA 08
1	SEA 5027
1	SEA 55W3 (Comstock)
1	SEA 55W31 (Jones)
1	SEA 56X7 (Crockett)
2	SEA 56Y11 (Saavedra)
2	SEA 56Y12 (Enatsky)
2	SEA 56Y13 (Wagner)
1	SEA 92R (DiGiovanni)
12	DTIC
2	University of Iowa, IIHR
1	L. Landweber
1	A.T. Chwang
2	Virginia Polytechnic Inst.
	Engineering Science & Mechanics
1	D. Walker
1	D.T. Mook

INITIAL DISTRIBUTION (continued)

Copies

1 Douglas Aircraft Co., Long Beach

1 J.L. Hess (Mail Code 212-10)

1 BBN Systems and Technologies Co.

1 M.S. Howe

1 United Technologies Res. Center

East Hartford

1 R.P. Dring

1 NASA Ames Res. Center

1 M.M. Rai (MS 258)

CENTER DISTRIBUTION

Copies	Code	Name
1	0113	Douglas
1	0114	
1	0115	
1	0117	Nakonechny
1	15	Morgan
1	1500	Goldstein
1	1506	Walden
1	1508	Boswell
1	154	McCarthy
1	1542	Huang
10	1542	Lee
1	1544	Peterson
1	1563	Moran
1	1564	Feldman
1	1905	Blake
1	1942	Hwang
1	1843	Cheng
1	27B	Cox
1	2704	Hwang
1	2704	Quandt
1	2704	Tang
1	272	Doyle
1	2720	Hatchard
1	2720	Kornbau
1	2720	Urbach
10	2721	Bein
1	2722	Helmick
1	2723	Stricker
1	2723	Becnel
1	274	Wang
1	2741	Henry
1	2741	Calvert
1	522.1	TIC (C)
1	522.1	TIC (C)
1	5231	Office Services

Copies	Code	Name
1	27	Argiro